JGR Atmospheres

RESEARCH ARTICLE
10.1029/2023JD038811

Stratosphere-Troposphere Coupling of Extreme Stratospheric Wave Activity in CMIP6 Models

Xiuyuan Ding[1], Gang Chen[1], and Weiming Ma[2]

[1]Department of Atmospheric and Oceanic Sciences, University of California, Los Angeles, CA, USA, [2]Atmospheric Sciences and Global Change Division, Pacific Northwest National Laboratory, Richland, WA, USA

Key Points:

- Increased risks of cold spells over North America follow strong stratospheric wave events or precede weak stratospheric wave events
- The vertical wave coupling during strong wave events features a shift of vertical wave phase line from westward tilt to eastward tilt
- Intermodel spread in stratospheric wave structure correlates with tropospheric circulation anomalies during strong wave events

Supporting Information:

Supporting Information may be found in the online version of this article.

Correspondence to:

X. Ding and G. Chen,
dingxy@ucla.edu;
gchenpu@ucla.edu

Citation:

Ding, X., Chen, G., & Ma, W. (2023). Stratosphere-troposphere coupling of extreme stratospheric wave activity in CMIP6 models. *Journal of Geophysical Research: Atmospheres*, *128*, e2023JD038811. https://doi.org/10.1029/2023JD038811

Received 2 MAR 2023
Accepted 4 AUG 2023

Abstract Extreme stratospheric wave activity has been suggested to be connected to surface temperature anomalies, but some key processes are not well understood. Using observations, we show that the stratospheric events featuring weaker-than-normal wave activity are associated with increased North American (NA) cold extreme risks before and near the event onset, accompanied by less frequent atmospheric river (AR) events on the west coast of the United States. Strong stratospheric wave events, on the other hand, exhibit a tropospheric weather regime transition. They are preceded by NA warm anomalies and increased AR frequency over the west coast, followed by increased risks of NA cold extremes and north-shifted ARs over the Atlantic. Moreover, these links between the stratosphere and troposphere are attributed to the vertical structure of wave coupling. Weak wave events show a wave structure of westward tilt with increasing altitudes, while strong wave events feature a shift from westward tilt to eastward tilt during their life cycle. This wave phase shift indicates vertical wave coupling and likely regional planetary wave reflection. Further examinations of CMIP6 models show that models with a degraded representation of stratospheric wave structure exhibit biases in the troposphere during strong wave events. Specifically, models with a stratospheric ridge weaker than the reanalysis exhibit a weaker tropospheric signal. Our findings suggest that the vertical coupling of extreme stratospheric wave activity should be evaluated in the model representation of stratosphere-troposphere coupling.

Plain Language Summary It is challenging to predict cold spells beyond 2 weeks due to chaotic weather systems. Taking into account stratospheric variability may push predictions beyond this limit. Previous studies have suggested that a stratospheric circulation pattern is connected to surface temperature. Strong and weak stratospheric wave events are defined based on the phase of this pattern. In observations, we find more frequent cold spells over North America and less precipitation over the west coast before and around weak wave events. On the other hand, strong wave events correspond to significant weather changes. Warmer weather over North America and more precipitation over the west coast occur before strong wave events, while more frequent cold spells over North America take place around 10 days later. We reveal that the weather changes during strong wave events correspond to a transition in the vertical structure of planetary waves. State-of-the-art climate models capture the overall linkage between stratospheric wave events and surface conditions. We further illustrate that the models incapable of simulating a realistic stratospheric wave pattern tend to show larger biases in the troposphere during strong wave events. Our findings urge the need to improve the stratospheric wave representation in climate models.

1. Introduction

It is widely recognized that stratospheric variability is connected to tropospheric weather conditions during boreal winter (e.g., Baldwin et al., 2021; Domeisen et al., 2020b; Sigmond et al., 2013). In the winter stratosphere, a powerful cyclonic system termed the polar vortex develops over the polar region as the result of large solar radiation gradients. The strength of a stratospheric polar vortex is also modulated by wave drag due to planetary waves propagating from the troposphere to the stratosphere (e.g., Charney & Drazin, 1961; Matsuno, 1970). Both weak and strong polar vortex events have been shown to influence the troposphere and surface on sub-seasonal to seasonal timescales (e.g., Baldwin & Dunkerton, 2001; Limpasuvan et al., 2004, 2005).

Several mechanisms are proposed for the stratospheric impacts on the surface, involving different aspects of the planetary wave-zonal flow interaction. Planetary waves propagate upwards into the stratosphere, where waves are absorbed and under certain conditions result in an extremely weak polar vortex, known as sudden stratospheric warming (SSW; Charney & Drazin, 1961; Garfinkel et al., 2010; Polvani & Waugh, 2004). Following

SSWs, downward propagation of negative zonal wind anomalies may be amplified and sustained by tropospheric synoptic eddy feedbacks (Domeisen et al., 2013; Gerber et al., 2010; Kushner & Polvani, 2004; Martineau et al., 2018; Song & Robinson, 2004; Sun et al., 2012). The surface signals of SSWs are characterized by the negative phase of the Arctic Oscillation (AO) or North Atlantic Oscillation (NAO) and more frequent cold spells in the mid-latitudes, particularly in northern Eurasia (Butler et al., 2017; Domeisen & Butler, 2020; Garfinkel et al., 2017; Hitchcock & Simpson, 2014; Kidston et al., 2015; Zhang et al., 2020). Another mechanism refers to planetary wave reflection in the stratosphere. Upward-propagating waves from the troposphere get reflected downwards and influence the tropospheric circulation (Perlwitz & Harnik, 2003; Shaw & Perlwitz, 2010). Planetary wave reflection events are linked to a strong stratospheric polar vortex and positive NAO at the surface (Kodera et al., 2013, 2016; Shaw & Perlwitz, 2013). Other mechanisms include the role of the residual circulation (Thompson et al., 2006; Yang et al., 2015), or modulation of tropical deep convection (Collimore et al., 2003; Gray et al., 2018; Liess & Geller, 2012). Moreover, various tropospheric precursors have been identified as the source of anomalous upward wave propagation (Davies, 1981; Garfinkel et al., 2010; Kolstad & Charlton-Perez, 2011; Schneidereit et al., 2017; Sun et al., 2012), including atmospheric blocking over Euro-Atlantic and Pacific (Martius et al., 2009; Nishii et al., 2011; Woollings et al., 2010), Arctic sea ice (Kim et al., 2014; Sun et al., 2015; Zhang et al., 2018, 2020), and El Niño-Southern Oscillation (ENSO) (Butler et al., 2014, 2016; Butler & Polvani, 2011; Domeisen et al., 2015, 2020a).

Planetary wave reflection events have drawn increasing attention recently due to their connection to North American (NA) cold spells (e.g., Kretschmer et al., 2018). Particularly, Cohen et al. (2021) argue that a stretched polar vortex in the lower stratosphere, characterized by its horizontal elongation, is linked to NA cold extremes such as the February 2021 Texas cold spell via wave reflection. An important feature of these reflection events is the negative eddy heat flux in the lower stratosphere, which indicates downward wave propagation. Negative extremes of zonal mean eddy heat flux are instantaneously linked to positive NAO and NA cooling, while positive eddy heat flux extremes are linked to negative NAO and Eurasian cooling (Dunn-Sigouin & Shaw, 2018; Shaw et al., 2014; Shaw & Perlwitz, 2013). Messori et al. (2022) further suggest that reflection events featured by regionally negative eddy heat flux relate to the tropospheric evolution from a Pacific Trough regime to an Alaskan Ridge regime, accompanied by a continental-scale temperature decrease over North America. However, Tan and Bao (2020) find no evidence of wave reflection linked with NA cold spells. They argue that the tropospheric circulation regime associated with NA cold spells only acts as a precursor for the suppressed planetary wave-1 (a wave structure with one crest and one trough at a latitude circle) activity in the stratosphere. Ding et al. (2022, 2023), in contrast, show that strong stratospheric wave activity precedes positive NAO-like NA cooling at the surface with a 10-day lag. The divergent conclusions underscore that the surface impacts of stratospheric waves remain an area of active research.

A key challenge in understanding stratosphere-troposphere coupling is the large internal variability in both the stratosphere and troposphere (Afargan-Gerstman et al., 2022; Charlton-Perez et al., 2018; Kolstad et al., 2022). Only about two-thirds of SSWs are followed by visible downward influences characterized by persistent negative AO, and less than a quarter of negative NAO events are preceded by an SSW (Domeisen, 2019). Davis et al. (2022) find that the February 2021 Texas cold spell is largely attributed to unpredictable internal atmospheric variability, with no discernible contribution from the stratosphere. To deal with the limited sample size of events, one approach is to use large ensembles of model simulations. In comparison with high-top models, low-top models are found to underestimate the SSW frequency (Charlton-Perez et al., 2013). Shaw et al. (2014) demonstrate that a degraded model representation of stratospheric eddy heat fluxes is linked to biases in the troposphere through downward wave coupling. Wu and Reichler (2020) further show that not only a high model lid but also a fine vertical resolution in the stratosphere is important for properly simulating stratospheric variability.

The role of extreme stratospheric wave events in NA cold extremes is also underexplored in climate models. One possible reason is the challenge in diagnosing these events consistently in different datasets. Previous studies have identified stratospheric wave events using eddy heat fluxes (Dunn-Sigouin & Shaw, 2015), time-integrated upward wave activity flux (Reichler & Jucker, 2022), clustered 100 hPa circulation patterns (Cohen et al., 2021; Kretschmer et al., 2018; Liang et al., 2022), or time-filtered 10 hPa circulation patterns (Shen et al., 2022). However, many of these studies only analyzed reanalyzes, and the sensitivities of these methods are unclear when applied to climate models. Ding et al. (2022) measure stratospheric wave activity with a simple metric based on the EOF analysis of the zonally asymmetric component of 10 hPa geopotential height, which can be readily applied to climate models. Ding et al. (2023) further show the impact of extreme stratospheric wave events on NA

cold spells consistently across reanalysis and Coupled Model Intercomparison Project Phase 6 (CMIP6) ensemble means. The present study will assess extreme stratospheric wave activity in CMIP6 models. We examine the stratosphere-troposphere coupling of extreme stratospheric wave activity, including the impacts on temperature and precipitation extremes. We also quantify the statistical relationship between stratospheric and tropospheric circulation anomalies in the CMIP6 model ensemble for the vertical wave coupling during strong wave events.

Besides the well-studied surface signatures of stratospheric variability, we will examine the frequency of Atmospheric rivers (ARs) that play an important role in the hydroclimate. ARs are narrow regions of strong horizontal water vapor transport, responsible for more than 90% of the poleward moisture transport at midlatitudes (Zhu & Newell, 1998). They can lead to extreme events including extreme precipitation (Ma et al., 2020), extreme wind events (Waliser & Guan, 2017) and flooding (Leung & Qian, 2009), particularly along the western coasts of North America and Europe. Recent studies show that anomalies in the strength of stratospheric polar vortex can influence the frequency of ARs and the associated precipitation through an anomalous tropospheric jet (Baek et al., 2023; Lee et al., 2022; Ma & Chen, 2022). However, given the distinct planetary wave mechanism and surface impacts, the potential influence of extreme stratospheric wave events on ARs remains elusive.

The paper is organized as follows. Section 2 describes the data, definition of stratospheric wave event, and AR detection. In Section 3, we analyze the linkages between stratospheric wave activity and tropospheric extremes in the reanalysis data. Section 4 examines the representation of stratospheric wave activity in CMIP6 models and its linkage to the troposphere. Section 5 draws a comparison between stratospheric wave events and several other types of stratospheric events. Section 6 provides a summary.

2. Data and Methods

2.1. Observations and CMIP6 Models

We use the fifth generation of atmospheric reanalysis from the European Center for Medium-Range Weather Forecasts (ERA5; Hersbach et al., 2020). The daily data we analyzed has a spatial resolution of 1.5° × 1.5°. We focus on the extended boreal winter from November to March over the period of 1950–2021. After detrending, we remove the seasonal cycle in the data, which is defined as the time mean and first two harmonics of the full-year climatology.

We also analyze the historical simulations from 30 CMIP6 models. The daily data covers the period of 1950–2014 (except that GISS-E2-2-G covers 1970–2014 due to limited data availability). All model data are bilinearly interpolated to a common grid of 1.5° × 1.5°. Only one member in each model ensemble is used. The list of CMIP6 models, the ensemble members used, and lid height are briefly summarized in Table S1 in Supporting Information S1. In addition to the CMIP6 ensemble, we examine another model ensemble by incorporating eight additional members of CESM2, constituting a 9-member CESM2 ensemble. Because each member of this CESM2 ensemble differs only by small perturbations to initial conditions, their differences are attributed to the internal variability of the climate system. We repeat the CMIP6 analysis with this 9-member ensemble to estimate the internal variability in CESM2.

2.2. Definition of Extreme Stratospheric Wave Events

We define extreme stratospheric wave events based on the EOF analysis of 10 hPa geopotential height for ERA5 and individual CMIP6 models, as in Ding et al. (2022). After removing the zonal mean, EOF is applied to the zonally asymmetric component of geopotential height at 10 hPa north of 20°N, weighted by the square root of the cosine of latitudes. The stratospheric planetary wave index is defined as the standardized principal component of the leading EOF mode. The positive/negative phase of the wave index largely describes the intensification/weakening of the planetary wave-1 in the stratosphere (Figure 1), due to constructive/destructive interference with the climatological wave-1 (Smith & Kushner, 2012). A weak stratospheric wave event is then defined as the consecutive days when the planetary wave index is below its fifth percentile, and a strong wave event is defined as the consecutive days when the index is above its 95th percentile. No minimum duration is required to detect an event. Day 0 refers to the first day that meets the event definition. Day −5 denotes 5 days before day 0, and day 5 indicates 5 days after day 0. This definition yields 89 weak wave events and 93 strong wave events out of 71 winters in ERA5 and on average 82 weak and 85 strong events out of 64 winters in 30 CMIP6 models. We

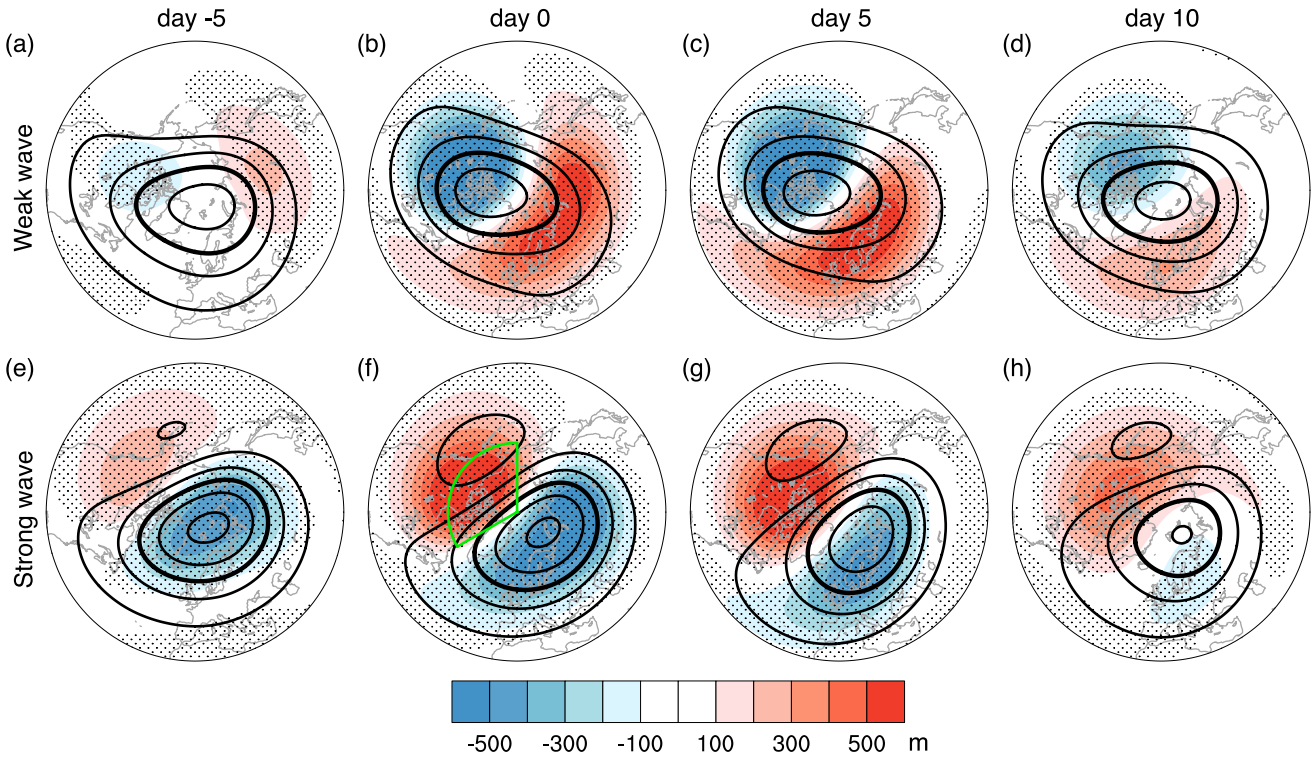

Figure 1. Composites of geopotential height at 10 hPa for weak (top) and strong (bottom) stratospheric wave events in the ERA5 reanalysis. (a and e) day −5, (b and f) day 0, (c and g) day 5, and (d and h) day 10. Shading denotes anomalies, and contours denote absolute values (contour intervals: 500 m) with 29,000 m contour emboldened. The time evolution is smoothed by a 5-day running average. Stippling represents the regions where the anomalies are significant at the 95% confidence level based on the Student's *t*-test. The green box (60°–90°N, 60°W–180°) in (f) indicates the region where stratospheric ridge anomalies are calculated.

note that the leading EOF pattern encompasses the variability from all zonal wave numbers and does not align perfectly with the climatological wave-1 pattern (Figure S1 in Supporting Information S1), hence a weak wave event may still produce a polar vortex stretching (Figure 1). Additionally, the third and fourth EOF patterns feature a wave-2 structure (Figure S2 in Supporting Information S1), which may also have important implications as previous studies have found an important role of wave-2 anomalies in split SSWs (Charlton & Polvani, 2007; Nakagawa & Yamazaki, 2006). However, since their explained variances (11.6% and 9.4%) are much smaller than that of the leading EOF (37.6%), we focus on the leading EOF in this study.

2.3. ARs and Precipitation in Observations

To quantify the stratospheric impact on hydrological extremes, we analyze the composites of ARs and precipitation for stratospheric wave events. We use the AR detection algorithm based on column integrated water vapor transport (IVT) developed by (Guan & Waliser, 2015). IVT is calculated by vertically integrating the moisture fluxes at 1,000, 850, 700, and 500 hPa. AR conditions are identified when IVT exceeds the seasonally and regionally dependent 85th percentile of IVT magnitude, with additional criteria on their spatial coherence, IVT direction, length, and length-to-width ratio. ARs are detected in 6-hourly data, but only 12:00 UTC AR data is used to calculate AR frequency to maintain the same daily resolution as the rest of our analysis.

The AR frequency, defined as the percentage of days when the above AR conditions are met at a grid point, is computed for 1979–2018 in ERA5. We also employ the daily accumulated precipitation estimate from Integrated Multi-satellitE Retrievals for GPM (IMERG; Huffman et al., 2014). The IMERG Final Run data covers the period from June 2000 to September 2021 with a spatial resolution of 1° × 1°. Because ARs and precipitation are available over shorter time spans, the AR composite is based on 52 out of 89 weak stratospheric wave events and 60 out of 93 strong wave events during 1979–2018, and the precipitation composite is based on 26 weak and 31 strong wave events during 2000–2021. As the result of fewer wave events, the composite analysis of weather extremes is averaged over a 15-day period before the wave event onset (i.e., days -15–0) or afterward (i.e., days 5–20), respectively.

2.4. Plumb Wave Activity Flux

The 3D Plumb wave activity flux is used to delineate planetary wave propagation. According to Plumb (1985), the Plumb flux is expressed as

$$\left\{F^{\lambda}, F^{\phi}, F^{z}\right\} = p\cos(\phi)\left\{v'^2 - \frac{1}{f\,a\cos(\phi)}\frac{\partial(v'\Phi')}{\partial\lambda}, -u'v' + \frac{1}{f\,a\cos(\phi)}\frac{\partial(u'\Phi')}{\partial\lambda}, \frac{f}{\partial\tilde{T}/\partial z + \kappa\tilde{T}/H}\left[v'T' - \frac{1}{f\,a\cos(\phi)}\frac{\partial(T'\Phi')}{\partial\lambda}\right]\right\}$$

where λ is longitude, ϕ is latitude, z is height, and p is pressure. T is temperature, Φ is geopotential height, u is the zonal wind, and v is the meridional wind. f is the Coriolis parameter and a is Earth's radius. κ is the specific gas constant of dry air divided by the specific heat of dry air. $\tilde{T}$ is the domain-averaged temperature. H is the log-pressure scale height. Primes denote the deviations from zonal means.

3. Linking Extreme Stratospheric Wave Activity With Weather Extremes in Reanalysis

3.1. Linkage Between Stratospheric Wave Activity and Surface Extremes

We begin by characterizing the evolution of the stratospheric circulation with respect to extreme stratospheric wave events. Figure 1 shows the composites of anomalous and total geopotential heights at 10 hPa for strong and weak wave events in the ERA5 reanalysis. For weak wave events, an anomalous trough over North America and an anomalous ridge over Eurasia are developed before day 0 and persist for about 5 days before they start to decay (Figures 1a–1d). The total geopotential height field features a polar vortex being stretched toward North America from day 0 to day 5 (also see Figure S3 in Supporting Information S1). The height anomalies of strong wave events are largely opposite to those of weak wave events, with a NA ridge and a Eurasian trough (Figures 1e–1h). The total geopotential height field shows a polar vortex displaced toward Eurasia, as compared with the vortex stretching for weak wave events (also see Figure S3 in Supporting Information S1). Notably, the wave-1 component of weak wave events is out of phase with the wave-1 climatology, while the wave-1 pattern of strong wave events is in phase with the climatology (Figure S1 in Supporting Information S1). In other words, the climatological wave-1 pattern is weakened via destructive interference between transient and climatological wave-1 during weak wave events, in contrast to the constructive wave interference during strong wave events (Smith & Kushner, 2012).

Figure 2 examines the corresponding tropospheric circulation of extreme stratospheric wave events. Before and around the onset of weak stratospheric wave events, 500 hPa geopotential height composites indicate a strong ridge around Alaska and two troughs over eastern North America and Europe, respectively (Figures 2a and 2b). This observed precursor pattern, reminiscent of the Alaskan Ridge weather regime over the NA sector (Lee et al., 2019; Vigaud et al., 2018), is similar to the tropospheric pattern associated with negative eddy heat flux events (see Figure 6 in Shaw & Perlwitz, 2013). It is worth noting that atmospheric blocking in this region has been recognized as a suppressor of upward wave propagation (e.g., Nishii et al., 2011). This convergence of findings highlights that these stratospheric events represent different aspects of the planetary wave-zonal flow interaction. From day 0 to day 10, this Alaskan ridge pattern evolves into a ridge over eastern North America and a trough over Siberia (Figure 2d). Note the dipole anomalies over the Atlantic from day 5 to day 10 project onto the negative phase of the NAO, which is opposite to the tropospheric pattern of negative eddy heat flux events (Shaw & Perlwitz, 2013).

The tropospheric circulation anomalies of strong stratospheric wave events are generally opposite to those of weak wave events. A trough occurs over Alaska and two ridges occur over eastern North America and Europe before and around the onset (Figures 2e and 2f). The precursor pattern of an Alaskan trough resembles the Pacific Trough weather regime over the NA sector (Lee et al., 2019; Vigaud et al., 2018). This is also consistent with the finding that a low-pressure anomaly over the North Pacific tends to enhance upward wave propagation, which serves as a precursor of SSWs (e.g., Garfinkel et al., 2010; Woollings et al., 2010). Around 10 days after the onset, a trough develops over Greenland and eastern North America, extending across the NA continent (Figure 2h). The dipole anomalies over the Atlantic strongly project onto positive NAO. The evolution of the tropospheric circulation during strong wave events resembles the transition associated with planetary wave reflection events

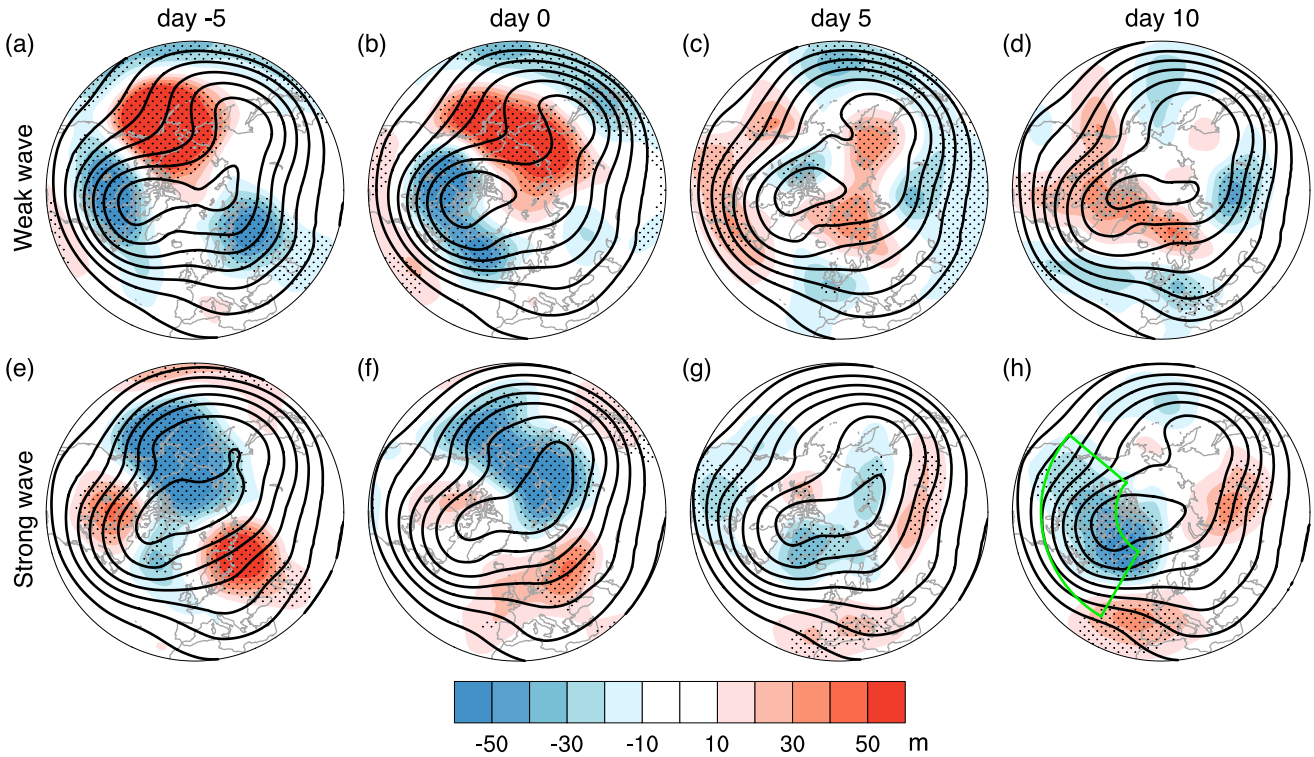

Figure 2. Composites of geopotential height at 500 hPa for weak (top) and strong (bottom) stratospheric wave events in ERA5 reanalysis. As in Figure 1, but for 500 hPa geopotential height. Shading denotes anomalies, and contours denote absolute values (contour intervals: 100 m). The green box (40°–70°N, 30°–130°W) in (h) indicates the region where tropospheric trough anomalies are calculated.

overall, but with no Alaskan ridge anomalies at positive lags (Messori et al., 2022). While the wave reflection events (Messori et al., 2022) are defined by the 100 hPa variability that may consist of both tropospheric and stratospheric variabilities, the stratospheric wave events defined here are based on 10 hPa and thus represent stratospheric variability.

Of particular interest is the linkage of stratospheric wave events with surface circulation and extremes. Figures 3a and 3d compare the composites of SAT and sea level pressure (SLP) anomalies before and after the onset of extreme stratospheric wave events. During days -15–0 of weak wave events, an anomalous positive SLP center over Alaska favors warm anomalies around the Bering Strait and cold anomalies over North America (Figure 3a). The NA cold anomalies are similar to the surface temperature signature observed during polar vortex stretching events (Cohen et al., 2021) and negative eddy heat flux events (Shaw et al., 2014). From day 5 to day 20, warm anomalies occur over eastern Canada and cold anomalies extend across northern Eurasia, consistent with the 500 hPa circulation patterns (Figures 2a–2d) and the SLP anomalies over the Atlantic that project onto negative NAO. In contrast, strong stratospheric wave events are preceded by cold anomalies around the Bering Strait and warm anomalies over North America, which are favored by deepened Aleutian Low before and near the onset (Figure 3d). We note that a deepened Aleutian Low has been long recognized as a precursor for a weak stratospheric polar vortex via constructive interference with the climatological wave-1 (Garfinkel et al., 2010; Nishii et al., 2011). For the period afterward, strong wave events are linked to extensive cold anomalies over North America, consistent with the anomalous trough at 500 hPa (Figures 2e–2h). The dipole in SLP anomalies over the Atlantic projects onto the positive phase of the NAO. This transition from NA warm anomalies to cold anomalies during strong wave events agrees with the lag regression analysis in Ding et al. (2022) and also the rapid temperature decrease over North America associated with wave reflection events in Messori et al. (2022). Although the magnitude of cold anomalies following strong stratospheric wave events is weaker than that of cold anomalies before or near the onset of weak wave events, strong wave events are particularly noteworthy because of the potential predictability for NA cold anomalies on subseasonal timescales.

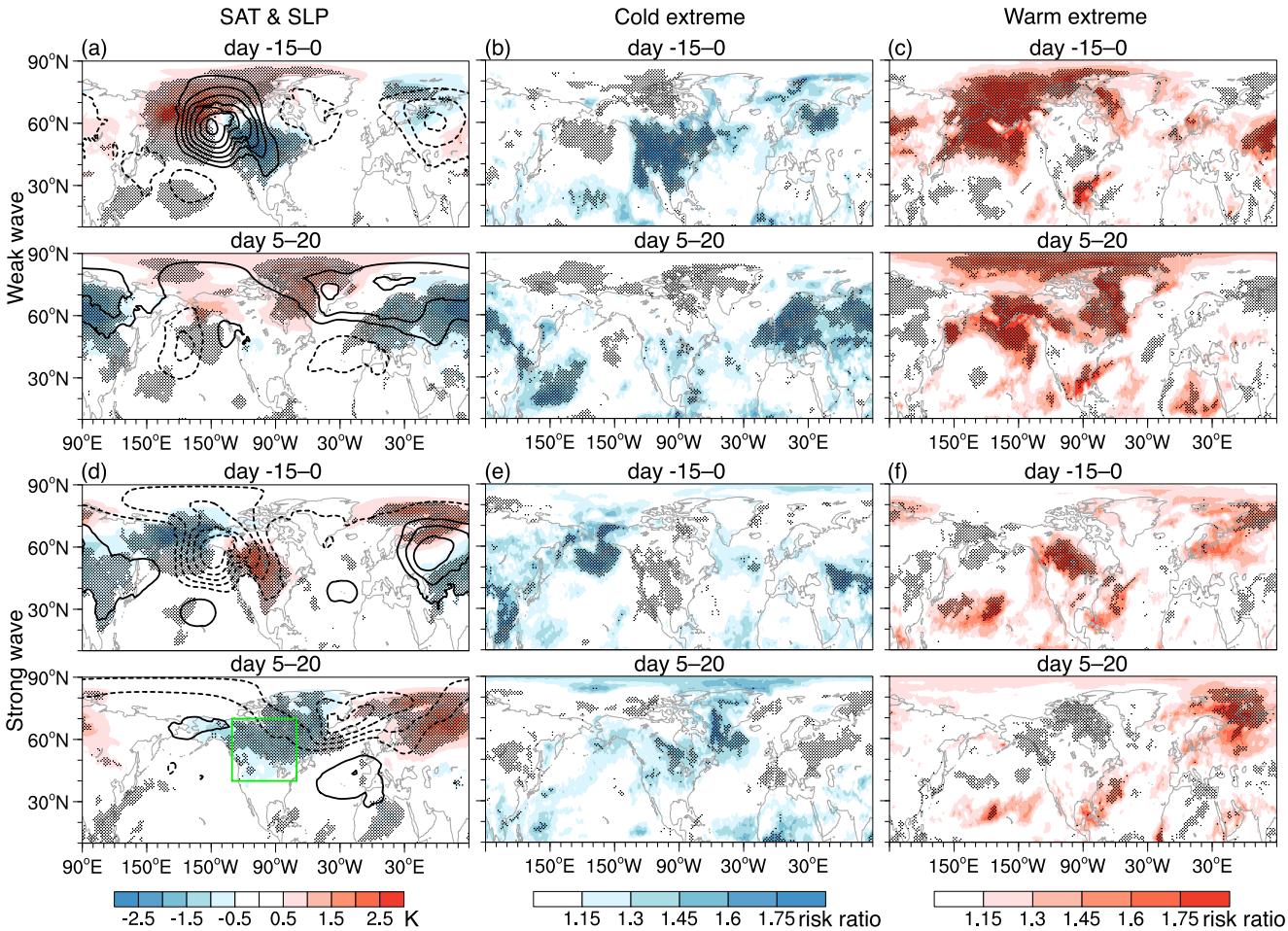

Figure 3. Composites of surface anomalies and SAT extremes for weak (top) and strong (bottom) stratospheric wave events in ERA5. (a and d) SAT anomalies in shading and SLP anomalies in contours (contour intervals: 1 hPa) during days -15–0 and during days 5–20. (b and e) the risk ratio of cold extremes during days -15–0 and during days 5–20. (c and f) the risk ratio of warm extremes during days -15–0 and during days 5–20. The risk ratio of cold (warm) extremes is defined as the probability of cold (warm) extreme days (SAT anomalies exceed 1.5 SD) during the period of interest divided by the probability of cold (warm) extreme days in all the winter days. Stippling represents the regions significant at the 95% confidence level based on the Student's *t*-test. The green box (40°–70°N, 70°–130°W) in (d) indicates the region where NA SAT anomalies are calculated.

Having illustrated the association between stratospheric wave activity and mean tropospheric conditions, we next discuss whether a similar linkage exists for daily surface temperature extremes. The impact of extreme stratospheric wave events on surface temperature extremes is quantified by the risk ratio of extreme cold and warm days. We define extreme cold/warm days when the SAT at a grid point lies at least 1.5 standard deviations (SD) below/above its climatology. The risk ratio of temperature extremes is measured as the ratio between the probability of temperature extremes associated with wave events and the probability of temperature extremes during all the winter days, with values larger than one indicating increased risks. From day −15 to day 0, weak wave events are associated with ∼60% higher risk of cold extremes across North America and over 75% higher risk of warm extremes over the northeast Pacific (Figures 3b and 3c). The increased risk of warm extremes persists with a smaller magnitude over the northeast Pacific during days 5–20, but the risk of cold extremes is elevated over Europe. For strong wave events, the risk of cold extremes increases over the northeast Pacific before and near the event onset, but the risk of warm extremes is enhanced over North America (Figures 3e and 3f). From day 5 to day 20, strong wave events enhance the risk of cold extremes by ∼30% across much of Canada and the Midwest United States, while the risk of warm extremes is enhanced over northern Europe. The risk ratio patterns of temperature extremes generally agree with the anomalous SAT composites (Figures 3a and 3d), suggesting that changes in temperature extremes may be explained by changes in mean temperature associated with stratospheric wave events.

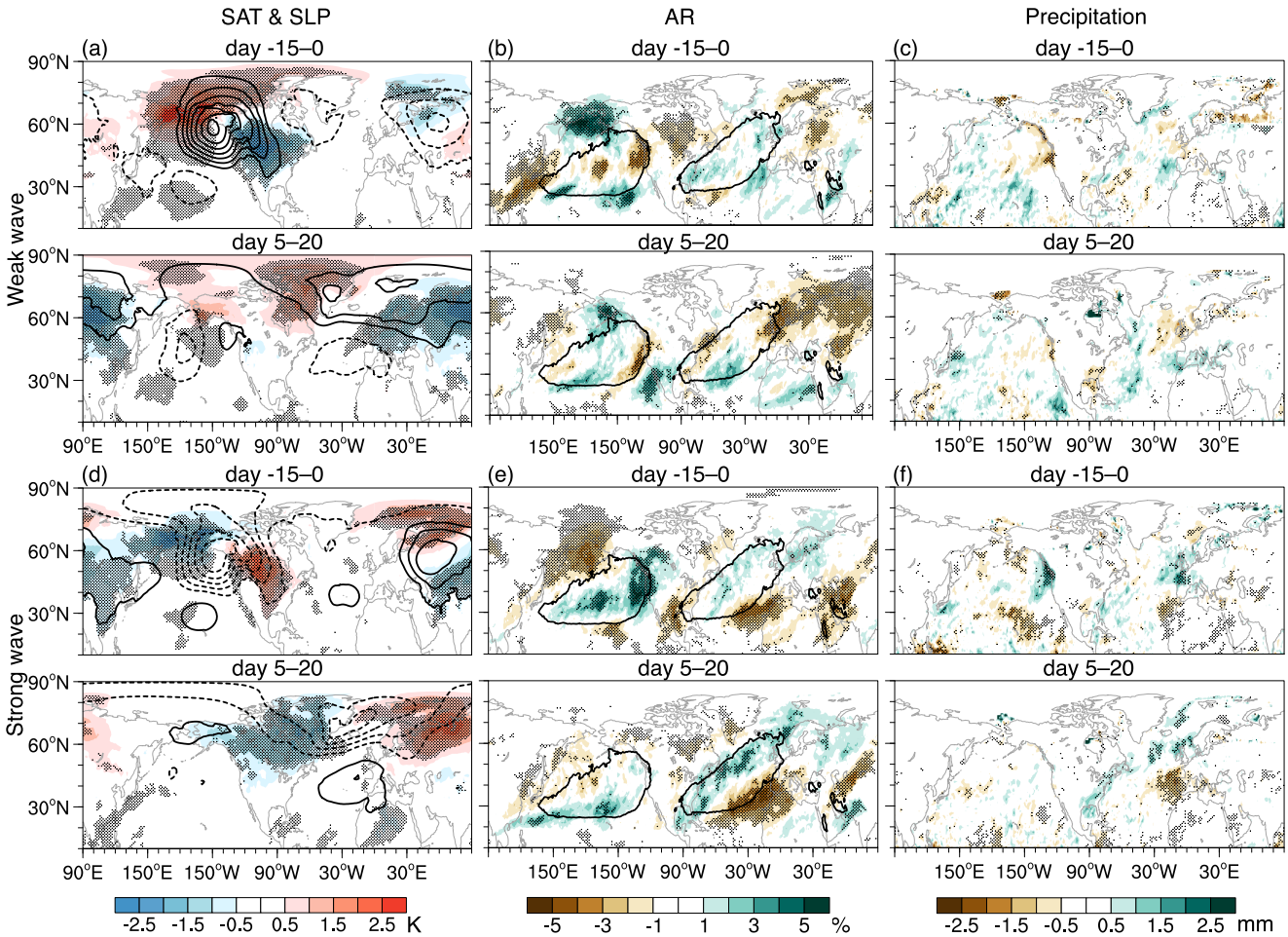

Figure 4. Composites of AR and precipitation anomalies for weak (top) and strong (bottom) stratospheric wave events in ERA5. (a and d) same as Figures 3a and 3d. (b and e) AR frequency anomalies during days -15–0 and during days 5–20. (c and f) precipitation anomalies during days -15–0 and during days 5–20. Contours in (b and e) denote regions where the climatological AR frequency exceeds 10%. Stippling represents the regions significant at the 95% confidence level based on the Student's *t*-test.

We further present anomalous AR frequency and anomalous precipitation before and after the extreme wave events (Figure 4). During days -15–0, weak wave events are preceded by reduced AR frequency along the center of the Pacific AR maximum region, accompanied by increased AR frequency on the north and south sides (Figure 4b). This tripole anomalous AR pattern resembles the second mode of interannual winter AR variability over the North Pacific identified in Ma and Chen (2022). This pattern is also consistent with the SLP anomalies of a strong positive center over the northeast Pacific and a secondary negative center to the south (Figure 4a). Correspondingly, precipitation decreases significantly along the west coast from 40°N to 60°N (Figure 4c), although no evident positive anomalies are observed on the northside possibly due to limited data coverage in IMERG north of 60°N. From day 5 to day 20, the AR anomalies over the Pacific weaken and shift slightly southwards. ARs become much less likely across the British Isles and Scandinavia, accompanied by reduced precipitation. This frequency decrease is likely attributed to the surface cooling and positive SLP anomaly over the north Atlantic (Figure 4a). Negative anomalies in temperature reduce the atmospheric moisture as governed by the Clausius-Clapeyron relation, resulting in reduced AR frequency and precipitation. Additionally, the positive SLP anomaly generates easterly wind anomalies and weakens onshore moisture transport along the Europe west coast, which also contributes to a reduction in AR frequency and precipitation.

In comparison with weak wave events, the anomalous patterns of strong wave events are generally of the opposite sign. Strong wave events are preceded by increased AR frequency over the Pacific AR maximum region, with reduced AR frequency on the north and south sides during days -15–0 (Figure 4e), consistent with the anomalous

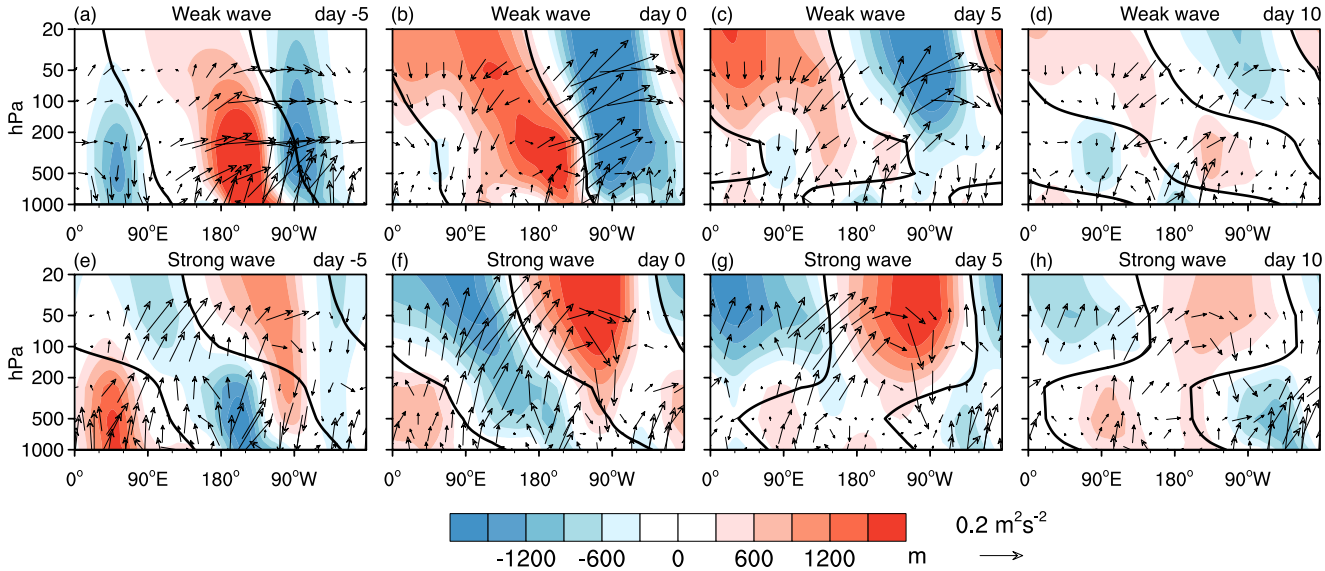

Figure 5. Vertical wave coupling during weak (top) and strong (bottom) wave events in ERA5. (a–d) composites of the zonally asymmetric component of anomalous geopotential height (shading) and the vertical and zonal components of anomalous Plumb wave activity flux (vector) averaged over 50°–70°N as a function of longitude and pressure on day −5, 0, 5, and 10 for weak wave events. (e–h) as in (a–d), but for strong wave events. Black lines are zero contours of the wave-1 component of anomalous geopotential height, indicating the phase tilt of wave-1. The time evolution is smoothed by a 5-day running average. To account for the smaller air density with decreasing pressure, the magnitude of the Plumb flux is scaled by $(1{,}000/p)^{1/2}$, and geopotential height is scaled by $(p/1{,}000)^{1/2}$, where p is pressure. The vertical component of the Plumb flux is also scaled by a factor of 200. See Figure S5 in Supporting Information S1 for the total (zonally asymmetric + zonal mean) field of anomalous geopotential height and absolute (anomalous + climatological) Plumb flux.

low-pressure center over the northeast Pacific (Figure 4d). This corresponds to the increase in precipitation along the west coast from 40°N to 60°N (Figure 4f). During days 5–20, ARs over the Atlantic are shifted poleward relative to the climatology, with increased frequency northside and decreased frequency southside of the AR maximum. Accordingly, precipitation increases over the British Isles and Scandinavia and decreases around the Iberian Peninsula (Figure 4f), consistent with a northward-shifted jet during positive NAO (Figure 4d). The anomalous AR patterns associated with the North Atlantic jet are largely consistent with the patterns of AR variability at seasonal or longer timescales (Baek et al., 2023; Lee et al., 2022; Ma & Chen, 2022).

3.2. Vertical Wave Structure During Extreme Stratospheric Wave Events

How is stratospheric wave activity connected to tropospheric variability? We examine the vertical structure of planetary wave coupling between the stratosphere and troposphere during extreme wave events in ERA5. Figure 5 displays the zonally asymmetric component of geopotential height anomalies and Plumb flux anomalies averaged over 50°–70°N during the life cycle of extreme stratospheric wave events. We note that the westward tilt of geopotential height anomalies with increasing altitude implies positive transient eddy heat fluxes that correspond to upward-propagating planetary waves, and that the Plumb fluxes include both transient eddy fluxes and the interference between transient and climatological planetary waves. For weak wave events, the westward tilt of the wave-1 phase line prevails through the life cycle, consistent with the wave-1 structure in the stratosphere around days -5–5 in Figure 1. After day 0, the tropospheric trough over North America quickly weakens and moves eastwards, leading to the termination of cold air advection and associated cold anomalies (Figure 3). Interestingly, the Plumb flux anomalies indicate downward wave activity fluxes over the eastern hemisphere from day 0 to day 5, due to the destructive interference between transient and climatological planetary waves.

Strong wave events show significant upward and eastward Plumb flux anomalies over Siberia, leading to the intensification of an anomalous stratospheric ridge over North America from day −5 to day 5 (Figures 5e–5g). As the stratospheric ridge intensifies and persists, the initial westward tilt of geopotential height anomalies transitions to an eastward tilt after day 0, indicating anomalous downward propagation of transient waves. This change in wave phase tilt is also evident for the wave-1 component alone, displayed in thick black lines. After the onset, the anomalous tropospheric ridge retrogrades westwards from the NA continent to the Pacific, yielding

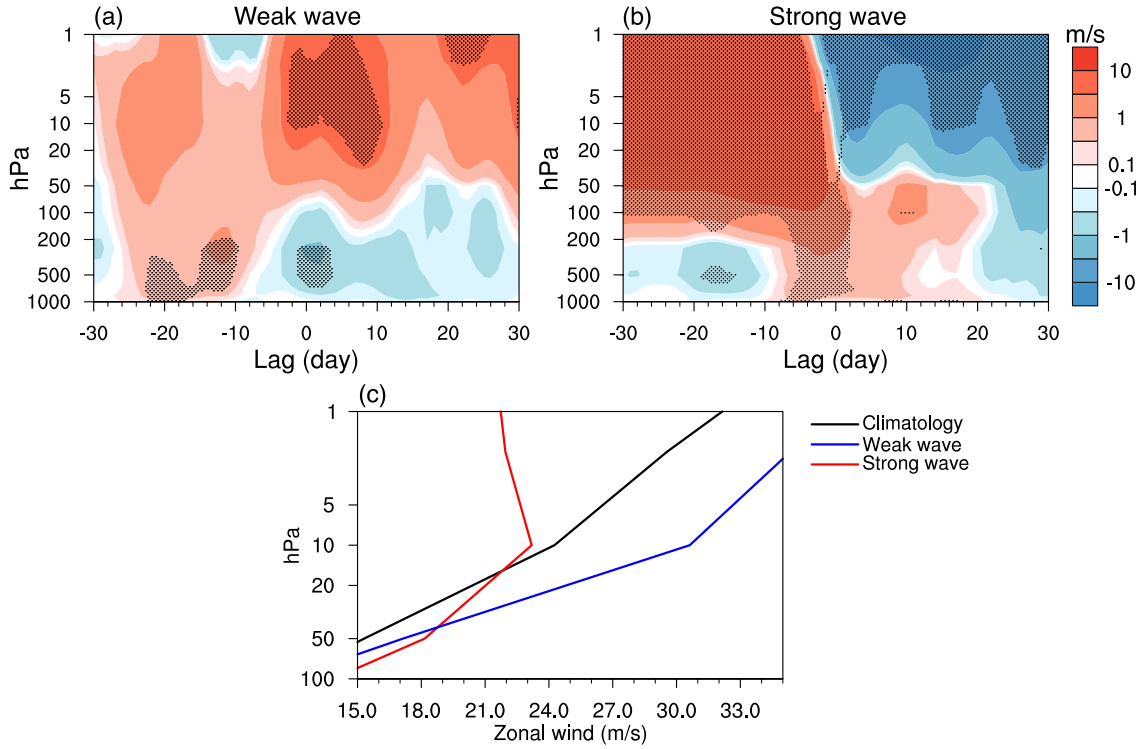

Figure 6. Zonally averaged high-latitude zonal wind for weak and strong wave events in ERA5. (a) Zonal wind anomalies averaged over 60°–80°N during weak wave events. (b) Zonal wind anomalies during strong wave events. A 5-day running average is applied. Stippling represents the regions where the anomalies are significant at the 95% confidence level based on the Student's *t*-test. (c) Absolute (anomalous + climatological) zonal wind profiles in the stratosphere averaged from day −2 to day 2.

an anomalous trough over eastern North America around days 5–10 (Figures 5g and 5h). This trough evolves in association with the SAT anomalies over North America (Figures 2 and 3). Moreover, the establishment of the tropospheric trough coincides with the downward Plumb flux anomalies over North America around days 0–10. These downward Plumb flux anomalies may be interpreted as local vertical wave reflection, although the zonal mean wave-1 eddy heat flux at 100 hPa remains positive throughout the strong wave events (Figure S4 in Supporting Information S1).

As previous studies suggest that the negative vertical zonal wind shear in the upper stratosphere may cause the vertical reflection of planetary waves (Perlwitz & Harnik, 2003), Figures 6a and 6b display the zonal wind anomalies averaged over 60°–80°N for extreme wave events in ERA5. Weak wave events show weakly positive zonal wind anomalies in the stratosphere from day 0 to day 10, which can be attributed to the weakening of the climatological wave-1 (Figures 1a–1d) and the reduced upward Plumb fluxes (Figure 5). And the negative zonal wind anomaly in the troposphere after day 0 coincides with the negative phase of the NAO (Figures 2 and 3). The zonal wind speed averaged around the weak wave event onset (blue line) increases with altitude in the stratosphere, similar to the climatological wind profile (Figure 6c). Strong wave events, however, feature a robust downward propagation of zonal wind anomalies (Figure 6b). A strong wind deceleration is observed around day 0 in the stratosphere, followed by positive anomalies in the troposphere which is consistent with positive NAO (Figures 2 and 3). More importantly, the stratospheric zonal wind speed (red line) decreases with altitude around the strong wave event onset (Figure 6c). This negative vertical zonal wind shear may indicate a vertical reflective surface for upward planetary wave propagation (Perlwitz & Harnik, 2003). Although the zonal mean eddy heat fluxes are positive, the presence of a vertical reflective surface and regionally downward Plumb fluxes (Figure 5 and S5 in Supporting Information S1) might hint at the role of local planetary wave reflection during strong wave events.

To summarize, the above analysis demonstrates an observed linkage between extreme stratospheric wave events and tropospheric temperature and precipitation. The tropospheric circulation patterns before and around the onset of these wave events align closely with known precursor patterns that either suppress or enhance upward planetary wave propagation, depending on the interference between transient waves and climatological waves (Garfinkel

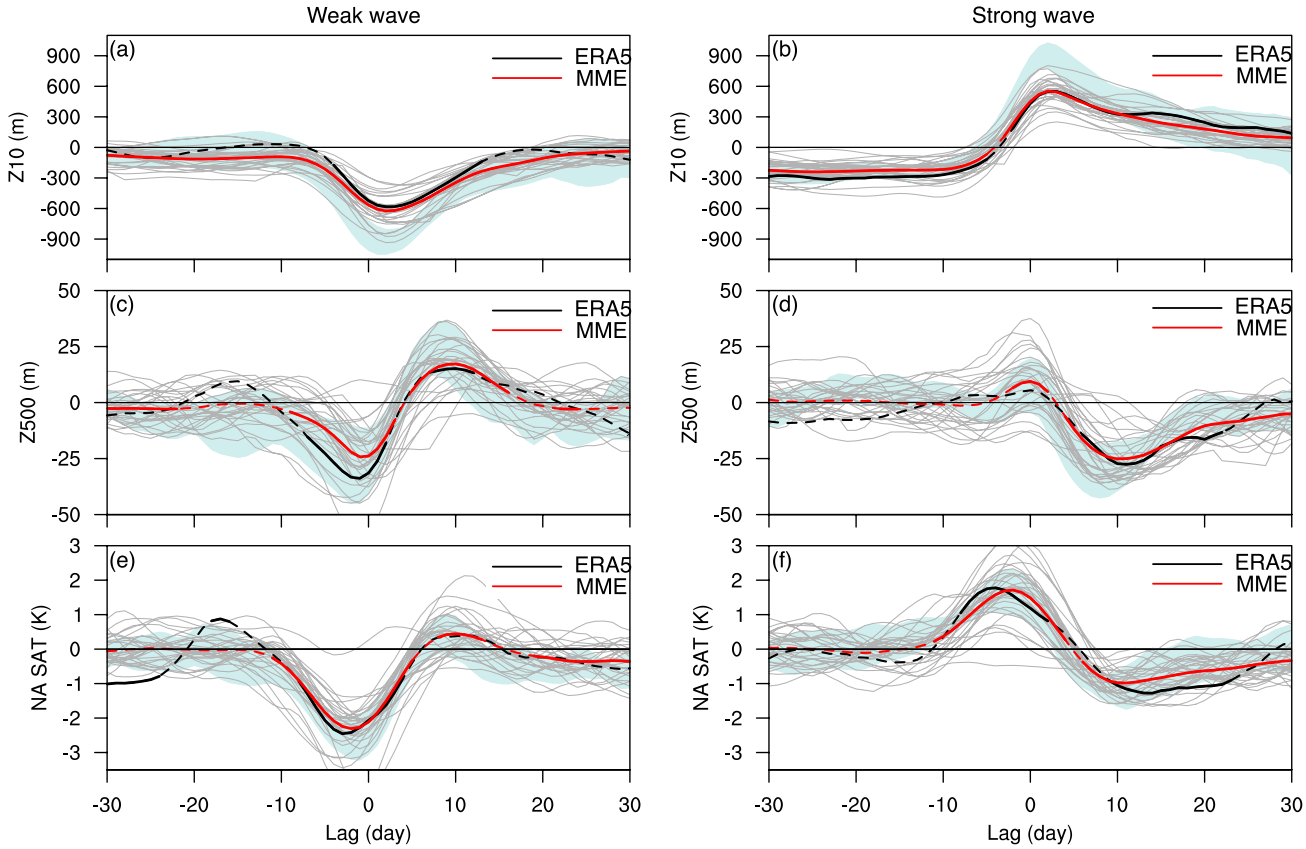

Figure 7. Evolution of circulation and NA SAT anomalies associated with weak (left) and strong (right) wave events in CMIP6 models. (a–b) 10 hPa geopotential height anomalies averaged over northern North America (60°–90°N, 60°W–180°). (c–d) 500 hPa geopotential height anomalies averaged over eastern North America (40°–70°N, 30°–130°W). (e–f) NA SAT anomalies averaged over land regions (40°–70°N, 70°–130°W). ERA5 is denoted by black lines, the CMIP6 multi-model ensemble (MME) mean is in red, and individual models are in light gray. Green shadings show the range across the 9-member CESM2 ensemble. The time evolution is smoothed by a 5-day running average. Solid parts of the lines for ERA5 and CMIP6 MME represent the anomalies significant at the 95% confidence level based on the Student's *t*-test.

et al., 2010; Nishii et al., 2011; Woollings et al., 2010). It is worth noting that the surface precursors of weak wave events exhibit similarities to the surface signals associated with wave reflection events (Cohen et al., 2021; Shaw et al., 2014). The strong stratospheric wave events are followed by an elevated risk of NA cold extremes and north-shifted ARs over the Atlantic, resulting in precipitation anomalies consistent with a northward-shifted jet during positive NAO. The analysis of the vertical structure corroborates the two-way coupling during these stratospheric wave events. These results suggest that extreme stratospheric wave activity has important implications for the predictability of tropospheric weather extremes on subseasonal timescales, warranting further evaluations of extreme stratospheric events in CMIP6 models.

4. Coupling Between Stratospheric Wave Activity and the Troposphere in CMIP6 Models

Figure 7 compares the temporal evolution of circulation and surface conditions associated with extreme stratospheric wave events in CMIP6 models. The time series of regionally averaged 10 hPa geopotential height anomalies over northern North America (60°–90°N, 60°W–180°) is compared with that of 500 hPa geopotential height anomalies over eastern North America (40°–70°N, 30°–130°W). The regions are selected based on the dominant circulation features in the stratosphere and troposphere (Figures 1 and 2). For weak wave events, an anomalous stratospheric trough over northern North America is developed and reaches a peak around day 2 (Figure 7a). This is preceded by an anomalous tropospheric trough that matures over eastern North America during days -10–0 and subsequently evolves into an anomalous ridge during days 5–20 (Figure 7c). The evolution of strong wave events is generally opposite to that of weak wave events (Figures 7b and 7d), except that the tropospheric trough

after the event onset is more persistent. The CMIP6 multi-model ensemble (MME) mean (red lines) agrees very well with ERA5 (black lines), implying that CMIP6 models can largely capture the physical processes at play for stratosphere-troposphere coupling of extreme stratospheric wave activity.

We next show the evolution of SAT anomalies associated with extreme wave events. We define NA SAT as the regional average of SAT over land regions within 40°–70°N, 70°–130°W, corresponding to the area of large SAT signals (Figures 3a and 3d). The evolution of NA SAT is very consistent with the regional circulation evolution (Figures 7c–7f), indicating that these NA SAT anomalies are likely caused by anomalous circulation. Weak wave events exhibit strong cold anomalies over North America before day 0, but these signals weaken rapidly after day 0 (Figure 7e). Strong wave events, in contrast, show a swing from warm anomalies around day −5 to cold anomalies around day 10 (Figure 7f), consistent with the temperature composite patterns in Figure 3d. The CMIP6 model results, albeit the large spread across models, agree with ERA5 on the swing from warm anomalies to cold anomalies in association with strong wave events, supporting the potential predictability for cold spells from strong stratospheric wave activity. In addition, we note that the inter-member spread within a single model (the 9-member CESM2 ensemble) (green shading) is smaller compared to the intermodel spread across CMIP6 models (gray lines), indicating that while internal atmospheric variability plays a role, systematic intermodel differences are an important contributor to the observed spread of the stratosphere-troposphere coupling of extreme stratospheric wave events.

We will hereafter focus on strong stratospheric wave events because they potentially benefit the subseasonal forecast of extreme cold events over North America. We notice a large uncertainty in the wave event evolution across CMIP6 models (Figure 7). Since the previous analysis has identified a linkage between the stratospheric ridge and tropospheric trough over North America during strong wave events, a question arises: can the intermodel differences in stratospheric waves help explain different tropospheric responses?

To quantify the connection between stratospheric wave representation and its tropospheric fingerprints during strong stratospheric wave events, Figure 8a presents the scatterplot of the stratospheric ridge anomaly during days -5–5 versus the tropospheric trough anomaly during days 5–20 across CMIP6 models. These time periods are selected based on the timing of the largest signals in Figure 7. There is a significant linear correlation ($r = -0.52$) between the stratospheric ridge and the tropospheric trough. This intermodel relation supports the proposed mechanism that the model representation of the stratospheric ridge over northern North America influences the tropospheric responses to strong wave events. The ERA5 result (black dot) lies within the intermodel spread, indicating that the modeled stratosphere-troposphere coupling during strong wave events is comparable to the reanalysis. The intermodel relation identified here suggests that the stratospheric wave structure can serve as a performance metric for assessing the stratosphere-troposphere coupling of strong wave events in models. Moreover, Figure 8b shows the scatterplot of the tropospheric trough anomaly versus NA SAT. The strong linear correlation ($r = 0.68$) between them confirms that the trough over North America is closely linked to the surface cold anomalies. It is thus tempting to ask whether a linear relation may also exist between the stratospheric ridge and NA SAT. However, Figure 8c suggests otherwise. The weak correlation between the stratospheric ridge and NA SAT indicates that the intermodel spreads of their correlations with the tropospheric trough largely cancel each other and result in a very small net effect.

It is worth noting that internal variability (red error bars) accounts for less than half of the intermodel spread for the stratospheric ridge and tropospheric trough associated with strong wave events, while the internal variability in the NA SAT may be comparable to the intermodel spread. More quantitatively, the variance of the stratospheric ridge in the CESM2 ensemble is 17.4% of the entire CMIP6 ensemble variance. And the variance of the tropospheric trough in the CESM2 ensemble accounts for 32.8% of the entire ensemble variance, while that ratio for NA SAT is 134.1%. The different fractions of internal variability may also help explain the small correlation between the stratospheric ridge and NA SAT.

5. Comparison With Eddy Heat Flux Events and Planetary Wave Reflection Events

In light of the similarity between the wave events discussed here and other extreme stratospheric events in the literature, we have analyzed whether the strong or weak stratospheric wave events overlap with eddy heat flux events (Dunn-Sigouin & Shaw, 2015) or planetary wave reflection events (Messori et al., 2022) in ERA5 (Figures 9a and 9b). According to Dunn-Sigouin and Shaw (2015), positive/negative eddy heat flux events are identified when the 50 hPa wave-1 eddy heat flux (60°–90°N) crosses the 95th/5th percentile from January to

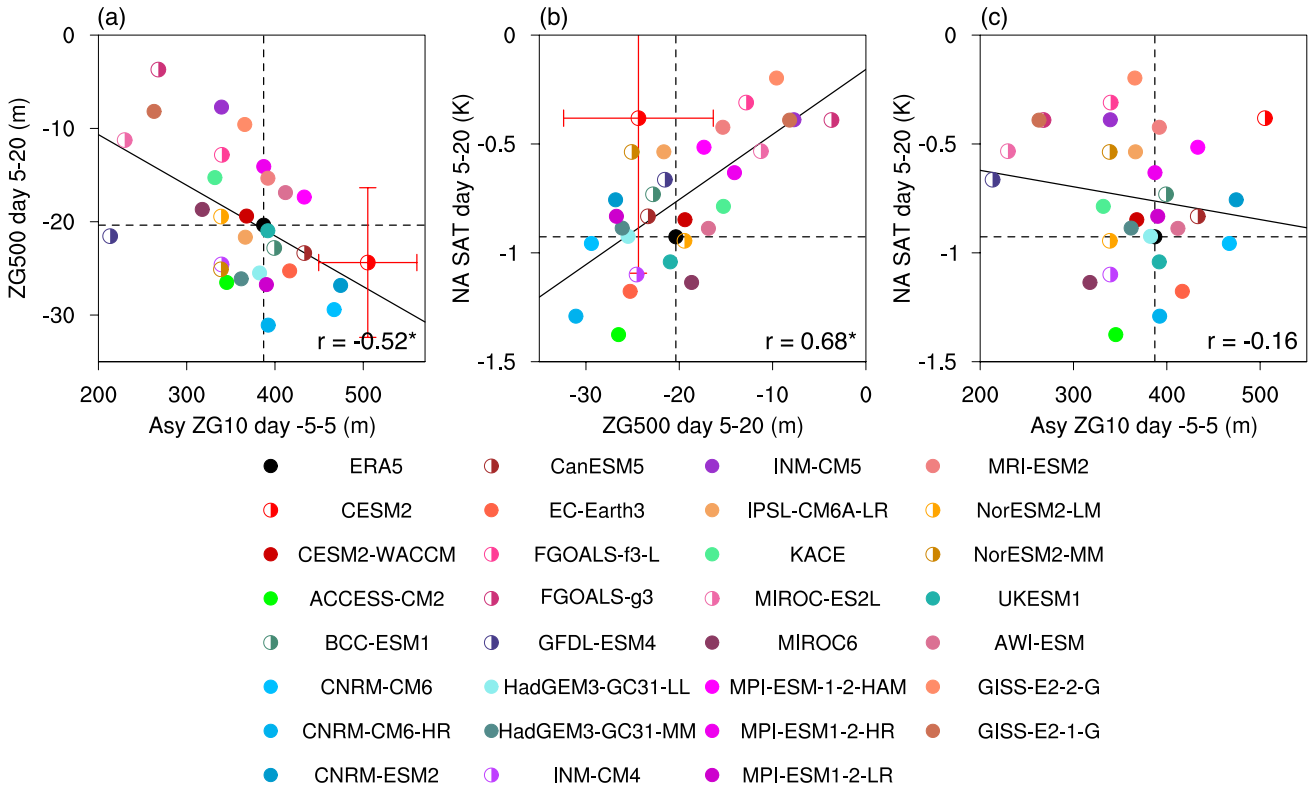

Figure 8. Intermodel spread of the relationship between stratospheric and tropospheric indices during strong wave events in CMIP6 models. (a) 10 hPa NA ridge during days −5–5 versus 500 hPa NA trough during days 5–20. (b) 500 hPa NA trough versus NA SAT during days 5–20. (c) 10 hPa NA ridge during days −5–5 versus NA SAT during days 5–20. 10 hPa NA ridge is defined by the asymmetric component of 10 hPa geopotential height anomalies over the northern NA region of 60°–90°N, 60°W–180°. 500 hPa NA trough is defined by 500 hPa geopotential height anomalies over the eastern NA region of 40°–70°N, 30°–130°W. Filled dots denote high-top models and half-filled dots indicate low-top models. The black lines show linear regressions for CMIP6 models, with correlation coefficients given in the legend. The red error bars show the ±2 SD in the 9-member CESM2 ensemble. Asterisks denote coefficients significant at the 95% confidence level based on the Student's *t*-test.

March. Day 0 is defined as the day of maximum or minimum heat flux. And events must be separated by at least 15 days. For the planetary wave reflection events, we use those dates from Messori et al. (2022).

Using a 15-day window centered at the onset of wave events defined in this study, we find that negative eddy heat flux events only occur in proximity to 13 of the 58 weak wave events during 1950–2021 (Figure 9a), and that positive heat flux events occur around 28 of the 67 strong wave events (Figure 9b). Note the numbers of stratospheric wave events are different from those in the previous sections because of the different time periods considered (November to March vs. January to March), which ensures a fair comparison across different stratospheric event types. And the planetary wave reflection events occur around 13 of the 45 strong wave events within 15 days around their onset during 1980–2021 based on the available dates of reflection events (Figure 9b). While all these stratospheric events feature significant NA temperature anomalies (Figures S6 and S7 in Supporting Information S1), weak wave events exhibit a stronger cold anomaly than negative eddy heat flux events (Figure 9c). Strong wave events show an overall similar NA SAT fingerprint as positive eddy heat flux events and planetary wave reflection events, with a transition from warm anomalies to cold anomalies (Figure 9d). Notably, strong wave events feature the most persistent cold anomalies that persist over 25 days after the event onset.

Additionally, in comparison to the dates of SSWs from the SSW Compendium data set (Butler et al., 2017), while some strong stratospheric wave events are followed by SSWs, many do not (Figure S8 in Supporting Information S1), suggesting strong stratospheric wave activity does not necessarily lead to SSWs. These findings align with previous studies which have found that strong wave flux may not be sufficient on its own to trigger an SSW (Cámara et al., 2017; Reichler & Jucker, 2022).

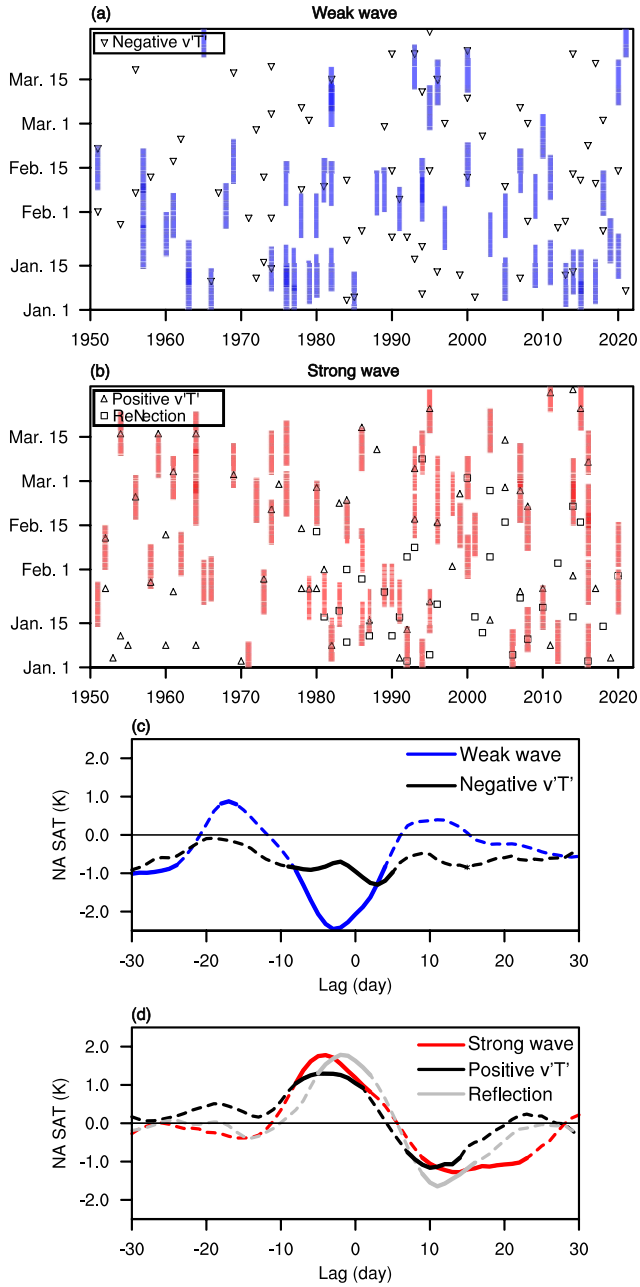

Figure 9. Dates of different stratospheric events and their composites of NA SAT in ERA5. (a) 15 days around the onset of weak wave events in shading. (b) as in (a), but for strong wave events. The dates of eddy heat flux events and planetary wave reflection events are denoted in the legend in (a)–(b). (c) composites of NA SAT for weak wave events (blue) and negative eddy heat flux events (black). (d) composites of NA SAT for strong wave events (red), positive heat flux events (black), and reflection events (gray). The time evolution in (c)–(d) is smoothed by a 5-day running average. Solid parts of the lines in (c)–(d) represent the anomalies significant at the 95% confidence level based on the Student's *t*-test.

6. Conclusion

In this paper, we investigate the vertical coupling of extreme stratospheric wave activity in ERA5 and CMIP6 models. Extreme stratospheric wave events are identified based on the EOF of the zonally asymmetric component of 10 hPa geopotential height. Weak wave events feature a horizontally stretched polar vortex in the stratosphere associated with the weakening of planetary wave-1, while strong wave events are characterized by a polar vortex displaced toward Eurasia accompanied by the amplification of wave-1 (Figure 1). In the troposphere, weak wave events are preceded by an anomalous NA trough and an Alaskan ridge, inducing intense surface cold anomalies over North America (Figures 2 and 3). Strong wave events, in contrast, are preceded by intensified Aleutian low with NA warming, transitioning into an anomalous NA trough with NA cooling and positive NAO around 10 days later. Here we highlight the lagged relation between strong stratospheric wave activity and NA surface cooling, with implications for subseasonal prediction of the NA cold events. Guan et al. (2020) suggest a similar role of stratosphere-troposphere coupling in a subseasonal NA temperature variability mode. The subseasonal swing in temperature also resembles the surface fingerprints of the stratosphere-troposphere oscillation identified by Shen et al. (2022). These are also in line with other recent studies that suggest a stratospheric source of subseasonal predictability for NA surface temperature variability (e.g., Ding et al., 2022, 2023; Messori et al., 2022).

We have also documented the tropospheric extremes associated with stratospheric wave activity (Figures 3 and 4). During days -15–0 of weak wave events, we find ~60% higher cold extreme risk over North America and over 75% higher warm extreme risk over the northeast Pacific, with reduced AR frequency and less precipitation over the west coast of the United States. Following the onset of weak wave events, increased cold extreme risk and decreased AR frequency are observed over Europe. On the other hand, strong wave events exhibit higher warm extreme risks over North America and higher cold extreme risks over the northeast Pacific during days -15–0, with more frequent AR events and increased precipitation observed along the west coast of the United States. These are in contrast to days 5–20 after the onset, during which strong wave events are associated with a significantly higher risk of cold extremes over North America and a northward shift of AR frequency and precipitation over the Atlantic. Similar rainfall anomalies over the west coast of the United States are reported when the stratospheric polar vortex over Eurasia is intensified and weakened, respectively (Liang et al., 2022). These analyses demonstrate a robust linkage of stratospheric wave activity to temperature and hydrological extremes in the troposphere.

We refer to the vertical structure of planetary waves to understand the linkage between stratospheric wave activity and tropospheric conditions (Figure 5). Weak wave events feature the development and decay of a Pacific ridge and a NA trough extending from the troposphere to the stratosphere. This wave-1 structure tilts westwards with altitude, indicating upward-propagating transient waves that interfere destructively with the climatological planetary wave in the stratosphere. Strong wave events, on the other hand, feature a persistent stratospheric ridge over North America. As the vertical wave phase shifts from a westward tilt before the event onset to an eastward tilt afterward, an anomalous trough develops over eastern North America in the troposphere. We also observe a reversal in the vertical shear of stratospheric zonal winds around the onset of strong wave events (Figure 6), suggesting a possible vertical reflective surface that may cause such a vertical phase shift (Perlwitz & Harnik, 2003). The shift in vertical wave phase tilt and the reflective surface may combine to indicate that planetary waves are regionally

reflected during strong wave events, but additional analysis is required due to the observed positive zonal mean eddy heat flux.

The stratosphere-troposphere coupling of extreme stratospheric wave events is further assessed in CMIP6 models. We explore the linkage between the stratospheric representation and tropospheric signals across individual models, finding a linear relationship between the strength of the stratospheric ridge and the strength of the following tropospheric trough over North America during strong stratospheric wave events (Figure 8a). This result suggests that the representation of stratospheric wave structure can serve as a metric to measure the vertical wave coupling of strong wave events. Future studies may wish to connect the representation of extreme wave events to certain aspects of model configurations, and if these configurations were to be refined, a better simulation of stratospheric or tropospheric variability may be expected from the improved vertical wave coupling. Finally, predictability studies may also investigate to what extent strong stratospheric wave events would improve weather forecasts on subseasonal timescales.

Conflict of Interest

The authors declare no conflicts of interest relevant to this study.

Data Availability Statement

The ERA5 reanalysis is available at https://www.ecmwf.int/en/forecasts/datasets/reanalysis-datasets/era5. The IMERG data can be downloaded from http://pmm.nasa.gov/data-access. The CMIP6 outputs used in this study can be obtained from the CMIP archive at https://esgf-node.llnl.gov/projects/esgf-llnl.

Acknowledgments
We thank three anonymous reviewers for their constructive comments that greatly improved the manuscript. We acknowledge the WCRP Working Group on Coupled Modeling which is responsible for the CMIP. We also acknowledge high-performance computing support from Cheyenne (https://doi.org/10.5065/D6RX99HX) provided by NCAR's Computational and Information Systems Laboratory, sponsored by the National Science Foundation. G.C. is supported by the U.S. NSF grant AGS-1832842 and AGS-2232581 and NASA Grant 80NSSC21K1522. W.M. acknowledges support by the U.S. Department of Energy (DOE), Office of Science, Office of Biological and Environmental Research, Regional and Global Model Analysis program area. The Pacific Northwest National Laboratory (PNNL) is operated for DOE by Battelle Memorial Institute under contract DE-AC05-76RLO1830.

References

Afargan-Gerstman, H., Jiménez-Esteve, B., & Domeisen, D. I. V. (2022). On the relative importance of stratospheric and tropospheric drivers for the North Atlantic jet response to sudden stratospheric warming events. *Journal of Climate*, *35*(19), 2851–6467. https://doi.org/10.1175/JCLI-D-21-0680.1

Baek, S. H., Battalio, J. M., & Lora, J. M. (2023). Atmospheric river variability over the last millennium driven by annular modes. *AGU Advances*, *4*(1), e2022AV000834. https://doi.org/10.1029/2022AV000834

Baldwin, M. P., Ayarzagüena, B., Birner, T., Butchart, N., Butler, A. H., Charlton-Perez, A. J., et al. (2021). Sudden stratospheric warmings. *Reviews of Geophysics*, *59*(1). https://doi.org/10.1029/2020RG000708

Baldwin, M. P., & Dunkerton, T. J. (2001). Stratospheric harbingers of anomalous weather regimes. *Science*, *294*(5542), 581–584. https://doi.org/10.1126/science.1063315

Butler, A. H., Arribas, A., Athanassiadou, M., Baehr, J., Calvo, N., Charlton-Perez, A., et al. (2016). The climate-system historical forecast project: Do stratosphere-resolving models make better seasonal climate predictions in boreal winter? *Quarterly Journal of the Royal Meteorological Society*, *142*(696), 1413–1427. https://doi.org/10.1002/qj.2743

Butler, A. H., & Polvani, L. M. (2011). El Niño, La Niña, and stratospheric sudden warmings: A reevaluation in light of the observational record. *Geophysical Research Letters*, *38*(13). https://doi.org/10.1029/2011GL048084

Butler, A. H., Polvani, L. M., & Deser, C. (2014). Separating the stratospheric and tropospheric pathways of El Niño–Southern oscillation teleconnections. *Environmental Research Letters*, *9*(2), 024014. https://doi.org/10.1088/1748-9326/9/2/024014

Butler, A. H., Sjoberg, J. P., Seidel, D. J., & Rosenlof, K. H. (2017). A sudden stratospheric warming compendium. *Earth System Science Data*, *9*(1), 63–76. https://doi.org/10.5194/essd-9-63-2017

Cámara, A. d. l., Albers, J. R., Birner, T., Garcia, R. R., Hitchcock, P., Kinnison, D. E., & Smith, A. K. (2017). Sensitivity of sudden stratospheric warmings to previous stratospheric conditions. *Journal of the Atmospheric Sciences*, *74*(9), 2857–2877. https://doi.org/10.1175/JAS-D-17-0136.1

Charlton, A. J., & Polvani, L. M. (2007). A new look at stratospheric sudden warmings. Part I: Climatology and modeling benchmarks. *Journal of Climate*, *20*(3), 449–469. https://doi.org/10.1175/JCLI3996.1

Charlton-Perez, A. J., Baldwin, M. P., Birner, T., Black, R. X., Butler, A. H., Calvo, N., et al. (2013). On the lack of stratospheric dynamical variability in low-top versions of the CMIP5 models. *Journal of Geophysical Research: Atmospheres*, *118*(6), 2494–2505. https://doi.org/10.1002/jgrd.50125

Charlton-Perez, A. J., Ferranti, L., & Lee, R. W. (2018). The influence of the stratospheric state on North Atlantic weather regimes. *Quarterly Journal of the Royal Meteorological Society*, *144*(713), 1140–1151. https://doi.org/10.1002/qj.3280

Charney, J. G., & Drazin, P. G. (1961). Propagation of planetary-scale disturbances from the lower into the upper atmosphere. *Journal of Geophysical Research (1896-1977)*, *66*(1), 83–109. https://doi.org/10.1029/JZ066i001p00083

Cohen, J., Agel, L., Barlow, M., Garfinkel, C. I., & White, I. (2021). Linking Arctic variability and change with extreme winter weather in the United States. *Science*, *373*(6559), 1116–1121. https://doi.org/10.1126/science.abi9167

Collimore, C. C., Martin, D. W., Hitchman, M. H., Huesmann, A., & Waliser, D. E. (2003). On the relationship between the QBO and tropical deep convection. *Journal of Climate*, *16*(15), 2552–2568. https://doi.org/10.1175/1520-0442(2003)016<2552:otrbtq>2.0.co;2;2

Davies, H. C. (1981). An interpretation of sudden warmings in terms of potential vorticity. *Journal of the Atmospheric Sciences*, *38*(2), 427–445. https://doi.org/10.1175/1520-0469(1981)038<0427:aioswi>2.0.co;2;2

Davis, N. A., Richter, J. H., Glanville, A. A., Edwards, J., & LaJoie, E. (2022). Limited surface impacts of the January 2021 sudden stratospheric warming. *Nature Communications*, *13*(1), 1136. https://doi.org/10.1038/s41467-022-28836-1

Ding, X., Chen, G., Sun, L., & Zhang, P. (2022). Distinct North American cooling signatures following the zonally symmetric and asymmetric modes of winter stratospheric variability. *Geophysical Research Letters*, *49*(6). https://doi.org/10.1029/2021GL096076

Ding, X., Chen, G., Zhang, P., Domeisen, D. I. V., & Orbe, C. (2023). Extreme stratospheric wave activity as harbingers of cold events over North America. *Communications Earth & Environment*, *4*(1), 1–10. https://doi.org/10.1038/s43247-023-00845-y

Domeisen, D. I. V. (2019). Estimating the frequency of sudden stratospheric warming events from surface observations of the North Atlantic Oscillation. *Journal of Geophysical Research: Atmospheres*, *124*(6), 3180–3194. https://doi.org/10.1029/2018JD030077

Domeisen, D. I. V., & Butler, A. H. (2020). Stratospheric drivers of extreme events at the Earth's surface. *Communications Earth & Environment*, *1*(1), 1–8. https://doi.org/10.1038/s43247-020-00060-z

Domeisen, D. I. V., Butler, A. H., Charlton-Perez, A. J., Ayarzagüena, B., Baldwin, M. P., Dunn-Sigouin, E., et al. (2020a). The role of the stratosphere in subseasonal to seasonal prediction: 1. Predictability of the stratosphere. *Journal of Geophysical Research: Atmospheres*, *125*(2), e2019JD030920. https://doi.org/10.1029/2019JD030920

Domeisen, D. I. V., Butler, A. H., Charlton-Perez, A. J., Ayarzagüena, B., Baldwin, M. P., Dunn-Sigouin, E., et al. (2020b). The role of the stratosphere in subseasonal to seasonal prediction: 2. Predictability arising from stratosphere-troposphere coupling. *Journal of Geophysical Research: Atmospheres*, *125*(2), e2019JD030923. https://doi.org/10.1029/2019JD030923

Domeisen, D. I. V., Butler, A. H., Fröhlich, K., Bittner, M., Müller, W. A., & Baehr, J. (2015). Seasonal predictability over Europe arising from El Niño and stratospheric variability in the MPI-ESM seasonal prediction system. *Journal of Climate*, *28*(1), 256–271. https://doi.org/10.1175/JCLI-D-14-00207.1

Domeisen, D. I. V., Sun, L., & Chen, G. (2013). The role of synoptic eddies in the tropospheric response to stratospheric variability. *Geophysical Research Letters*, *40*(18), 4933–4937. https://doi.org/10.1002/grl.50943

Dunn-Sigouin, E., & Shaw, T. A. (2015). Comparing and contrasting extreme stratospheric events, including their coupling to the tropospheric circulation. *Journal of Geophysical Research: Atmospheres*, *120*(4), 1374–1390. https://doi.org/10.1002/2014JD022116

Dunn-Sigouin, E., & Shaw, T. A. (2018). Dynamics of extreme stratospheric negative heat flux events in an idealized model. *Journal of the Atmospheric Sciences*, *75*(10), 3521–3540. https://doi.org/10.1175/JAS-D-17-0263.1

Garfinkel, C. I., Hartmann, D. L., & Sassi, F. (2010). Tropospheric precursors of anomalous northern hemisphere stratospheric polar vortices. *Journal of Climate*, *23*(12), 3282–3299. https://doi.org/10.1175/2010JCLI3010.1

Garfinkel, C. I., Son, S.-W., Song, K., Aquila, V., & Oman, L. D. (2017). Stratospheric variability contributed to and sustained the recent hiatus in Eurasian winter warming. *Geophysical Research Letters*, *44*(1), 374–382. https://doi.org/10.1002/2016GL072035

Gerber, E. P., Baldwin, M. P., Akiyoshi, H., Austin, J., Bekki, S., Braesicke, P., et al. (2010). Stratosphere-troposphere coupling and annular mode variability in chemistry-climate models. *Journal of Geophysical Research*, *115*, D00M06. https://doi.org/10.1029/2009JD013770

Gray, L. J., Anstey, J. A., Kawatani, Y., Lu, H., Osprey, S., & Schenzinger, V. (2018). Surface impacts of the Quasi biennial oscillation. *Atmospheric Chemistry and Physics*, *18*(11), 8227–8247. https://doi.org/10.5194/acp-18-8227-2018

Guan, B., & Waliser, D. E. (2015). Detection of atmospheric rivers: Evaluation and application of an algorithm for global studies. *Journal of Geophysical Research: Atmospheres*, *120*(24), 12514–12535. https://doi.org/10.1002/2015JD024257

Guan, W., Jiang, X., Ren, X., Chen, G., Lin, P., & Lin, H. (2020). The leading intraseasonal variability mode of wintertime surface air temperature over the North American Sector. *Journal of Climate*, *33*(21), 9287–9306. https://doi.org/10.1175/JCLI-D-20-0096.1

Hersbach, H., Bell, B., Berrisford, P., Hirahara, S., Horányi, A., Muñoz-Sabater, J., et al. (2020). The ERA5 global reanalysis. *Quarterly Journal of the Royal Meteorological Society*, *146*(730), 1999–2049. https://doi.org/10.1002/qj.3803

Hitchcock, P., & Simpson, I. R. (2014). The downward influence of stratospheric sudden warmings. *Journal of the Atmospheric Sciences*, *71*(10), 3856–3876. https://doi.org/10.1175/JAS-D-14-0012.1

Huffman, G. J., Bolvin, D. T., Braithwaite, D., Hsu, K., Joyce, R., Kidd, C., et al. (2014). Integrated multi-satellitE Retrievals for GPM (IMERG), version 4.4. *NASA's Precipitation Processing Center*. http://arthurhou.pps.eosdis.nasa.gov/gpmdata/

Kidston, J., Scaife, A. A., Hardiman, S. C., Mitchell, D. M., Butchart, N., Baldwin, M. P., & Gray, L. J. (2015). Stratospheric influence on tropospheric jet streams, storm tracks and surface weather. *Nature Geoscience*, *8*(6), 433–440. https://doi.org/10.1038/ngeo2424

Kim, B.-M., Son, S.-W., Min, S.-K., Jeong, J.-H., Kim, S.-J., Zhang, X., et al. (2014). Weakening of the stratospheric polar vortex by Arctic sea-ice loss. *Nature Communications*, *5*(1), 4646. https://doi.org/10.1038/ncomms5646

Kodera, K., Mukougawa, H., & Fujii, A. (2013). Influence of the vertical and zonal propagation of stratospheric planetary waves on tropospheric blockings. *Journal of Geophysical Research: Atmospheres*, *118*(15), 8333–8345. https://doi.org/10.1002/jgrd.50650

Kodera, K., Mukougawa, H., Maury, P., Ueda, M., & Claud, C. (2016). Absorbing and reflecting sudden stratospheric warming events and their relationship with tropospheric circulation. *Journal of Geophysical Research: Atmospheres*, *121*(1), 80–94. https://doi.org/10.1002/2015JD023359

Kolstad, E. W., & Charlton-Perez, A. J. (2011). Observed and simulated precursors of stratospheric polar vortex anomalies in the Northern Hemisphere. *Climate Dynamics*, *37*(7), 1443–1456. https://doi.org/10.1007/s00382-010-0919-7

Kolstad, E. W., Lee, S. H., Butler, A. H., Domeisen, D. I. V., & Wulff, C. O. (2022). Diverse surface signatures of stratospheric polar vortex anomalies. *Journal of Geophysical Research: Atmospheres*, *127*(20). https://doi.org/10.1029/2022JD037422

Kretschmer, M., Cohen, J., Matthias, V., Runge, J., & Coumou, D. (2018). The different stratospheric influence on cold-extremes in Eurasia and North America. *Npj Climate and Atmospheric Science*, *1*(1), 44. https://doi.org/10.1038/s41612-018-0054-4

Kushner, P. J., & Polvani, L. M. (2004). Stratosphere–troposphere coupling in a relatively simple AGCM: The role of eddies. *Journal of Climate*, *17*(3), 629–639. https://doi.org/10.1175/1520-0442(2004)017<0629:SCIARS>2.0.CO;2

Lee, S. H., Furtado, J. C., & Charlton-Perez, A. J. (2019). Wintertime North American weather regimes and the arctic stratospheric polar vortex. *Geophysical Research Letters*, *46*(24), 14892–14900. https://doi.org/10.1029/2019GL085592

Lee, S. H., Polvani, L. M., & Guan, B. (2022). Modulation of atmospheric rivers by the arctic stratospheric polar vortex. *Geophysical Research Letters*, *49*(18), e2022GL100381. https://doi.org/10.1029/2022GL100381

Leung, L. R., & Qian, Y. (2009). Atmospheric rivers induced heavy precipitation and flooding in the western U.S. simulated by the WRF regional climate model. *Geophysical Research Letters*, *36*(3). https://doi.org/10.1029/2008GL036445

Liang, Z., Rao, J., Guo, D., Lu, Q., & Shi, C. (2022). Northern winter stratospheric polar vortex regimes and their possible influence on the extratropical troposphere. *Climate Dynamics*, *60*(9–10), 3167–3186. https://doi.org/10.1007/s00382-022-06494-9

Liess, S., & Geller, M. A. (2012). On the relationship between QBO and distribution of tropical deep convection. *Journal of Geophysical Research*, *117*(D3). https://doi.org/10.1029/2011JD016317

Limpasuvan, V., Hartmann, D. L., Thompson, D. W. J., Jeev, K., & Yung, Y. L. (2005). Stratosphere-troposphere evolution during polar vortex intensification. *Journal of Geophysical Research*, *110*(D24), D24101. https://doi.org/10.1029/2005JD006302

Limpasuvan, V., Thompson, D. W. J., & Hartmann, D. L. (2004). The life cycle of the Northern Hemisphere sudden stratospheric warmings. *Journal of Climate*, *17*(13), 2584–2596. https://doi.org/10.1175/1520-0442(2004)017<2584:TLCOTN>2.0.CO;2

Ma, W., & Chen, G. (2022). What controls the interannual variability of the boreal winter atmospheric river activities over the Northern Hemisphere? *Journal of Climate*, *35*(23), 3955–7573. https://doi.org/10.1175/JCLI-D-22-0089.1

Ma, W., Chen, G., & Guan, B. (2020). Poleward shift of atmospheric rivers in the Southern Hemisphere in recent decades. *Geophysical Research Letters*, *47*(21), e2020GL089934. https://doi.org/10.1029/2020GL089934

Martineau, P., Chen, G., Son, S.-W., & Kim, J. (2018). Lower-stratospheric control of the frequency of sudden stratospheric warming events. *Journal of Geophysical Research: Atmospheres*, *123*(6), 3051–3070. https://doi.org/10.1002/2017JD027648

Martius, O., Polvani, L. M., & Davies, H. C. (2009). Blocking precursors to stratospheric sudden warming events. *Geophysical Research Letters*, *36*(14), L14806. https://doi.org/10.1029/2009GL038776

Matsuno, T. (1970). Vertical propagation of stationary planetary waves in the winter Northern Hemisphere. *Journal of the Atmospheric Sciences*, *27*(6), 871–883. https://doi.org/10.1175/1520-0469(1970)027<0871:vpospw>2.0.co;2;2

Messori, G., Kretschmer, M., Lee, S. H., & Wendt, V. (2022). Stratospheric downward wave reflection events modulate North American weather regimes and cold spells. *Weather and Climate Dynamics*, *3*(4), 1215–1236. https://doi.org/10.5194/wcd-3-1215-2022

Nakagawa, K. I., & Yamazaki, K. (2006). What kind of stratospheric sudden warming propagates to the troposphere? *Geophysical Research Letters*, *33*(4), L04801. https://doi.org/10.1029/2005GL024784

Nishii, K., Nakamura, H., & Orsolini, Y. J. (2011). Geographical dependence observed in blocking high influence on the stratospheric variability through enhancement and suppression of upward planetary-wave propagation. *Journal of Climate*, *24*(24), 6408–6423. https://doi.org/10.1175/JCLI-D-10-05021.1

Perlwitz, J., & Harnik, N. (2003). Observational evidence of a stratospheric influence on the troposphere by planetary wave reflection. *Journal of Climate*, *16*(18), 3011–3026. https://doi.org/10.1175/1520-0442(2003)016<3011:OEOASI>2.0.CO;2

Plumb, R. A. (1985). On the three-dimensional propagation of stationary waves. *Journal of the Atmospheric Sciences*, *42*(3), 217–229. https://doi.org/10.1175/1520-0469(1985)042<0217:OTTDPO>2.0.CO;2

Polvani, L. M., & Waugh, D. W. (2004). Upward wave activity flux as a precursor to extreme stratospheric events and subsequent anomalous surface weather regimes. *Journal of Climate*, *17*(18), 3548–3554. https://doi.org/10.1175/1520-0442(2004)017<3548:UWAFAA>2.0.CO;2

Reichler, T., & Jucker, M. (2022). Stratospheric wave driving events as an alternative to sudden stratospheric warmings. *Weather and Climate Dynamics*, *3*(2), 659–677. https://doi.org/10.5194/wcd-3-659-2022

Schneidereit, A., Peters, D. H. W., Grams, C. M., Quinting, J. F., Keller, J. H., Wolf, G., et al. (2017). Enhanced tropospheric wave forcing of two anticyclones in the prephase of the January 2009 major stratospheric sudden warming event. *Monthly Weather Review*, *145*(5), 1797–1815. https://doi.org/10.1175/MWR-D-16-0242.1

Shaw, T. A., & Perlwitz, J. (2010). The impact of stratospheric model configuration on planetary-scale waves in Northern Hemisphere winter. *Journal of Climate*, *23*(12), 3369–3389. https://doi.org/10.1175/2010JCLI3438.1

Shaw, T. A., & Perlwitz, J. (2013). The life cycle of Northern Hemisphere downward wave coupling between the stratosphere and troposphere. *Journal of Climate*, *26*(5), 1745–1763. https://doi.org/10.1175/JCLI-D-12-00251.1

Shaw, T. A., Perlwitz, J., & Weiner, O. (2014). Troposphere-stratosphere coupling: Links to North Atlantic weather and climate, including their representation in CMIP5 models. *Journal of Geophysical Research: Atmospheres*, *119*(10), 5864–5880. https://doi.org/10.1002/2013JD021191

Shen, X., Wang, L., Scaife, A. A., Hardiman, S. C., & Xu, P. (2022). The stratosphere-troposphere oscillation as the dominant intraseasonal coupling mode between the stratosphere and troposphere. *Journal of Climate*, *1*(aop), 1–41. https://doi.org/10.1175/JCLI-D-22-0238.1

Sigmond, M., Scinocca, J. F., Kharin, V. V., & Shepherd, T. G. (2013). Enhanced seasonal forecast skill following stratospheric sudden warmings. *Nature Geoscience*, *6*(2), 98–102. https://doi.org/10.1038/ngeo1698

Smith, K. L., & Kushner, P. J. (2012). Linear interference and the initiation of extratropical stratosphere-troposphere interactions. *Journal of Geophysical Research*, *117*(D13). https://doi.org/10.1029/2012JD017587

Song, Y., & Robinson, W. A. (2004). Dynamical mechanisms for stratospheric influences on the troposphere. *Journal of the Atmospheric Sciences*, *61*(14), 1711–1725. https://doi.org/10.1175/1520-0469(2004)061<1711:DMFSIO>2.0.CO;2

Sun, L., Deser, C., & Tomas, R. A. (2015). Mechanisms of stratospheric and tropospheric circulation response to projected Arctic Sea ice loss. *Journal of Climate*, *28*(19), 7824–7845. https://doi.org/10.1175/JCLI-D-15-0169.1

Sun, L., Robinson, W. A., & Chen, G. (2012). The predictability of stratospheric warming events: More from the troposphere or the stratosphere? *Journal of the Atmospheric Sciences*, *69*(2), 768–783. https://doi.org/10.1175/JAS-D-11-0144.1

Tan, X., & Bao, M. (2020). Linkage between a dominant mode in the lower stratosphere and the western Hemisphere circulation pattern. *Geophysical Research Letters*, *47*(17). https://doi.org/10.1029/2020GL090105

Thompson, D. W. J., Furtado, J. C., & Shepherd, T. G. (2006). On the tropospheric response to anomalous stratospheric wave drag and radiative heating. *Journal of the Atmospheric Sciences*, *63*(10), 2616–2629. https://doi.org/10.1175/JAS3771.1

Vigaud, N., Robertson, A. W., & Tippett, M. K. (2018). Predictability of recurrent weather regimes over North America during winter from submonthly reforecasts. *Monthly Weather Review*, *146*(8), 2559–2577. https://doi.org/10.1175/MWR-D-18-0058.1

Waliser, D., & Guan, B. (2017). Extreme winds and precipitation during landfall of atmospheric rivers. *Nature Geoscience*, *10*(3), 179–183. https://doi.org/10.1038/ngeo2894

Woollings, T., Charlton-Perez, A., Ineson, S., Marshall, A. G., & Masato, G. (2010). Associations between stratospheric variability and tropospheric blocking. *Journal of Geophysical Research*, *115*(D6), D06108. https://doi.org/10.1029/2009JD012742

Wu, Z., & Reichler, T. (2020). Variations in the frequency of stratospheric sudden warmings in CMIP5 and CMIP6 and possible causes. *Journal of Climate*, *33*(23), 10305–10320. https://doi.org/10.1175/JCLI-D-20-0104.1

Yang, H., Sun, L., & Chen, G. (2015). Separating the mechanisms of transient responses to stratospheric ozone depletion–like cooling in an idealized atmospheric model. *Journal of the Atmospheric Sciences*, *72*(2), 763–773. https://doi.org/10.1175/JAS-D-13-0353.1

Zhang, P., Wu, Y., Chen, G., & Yu, Y. (2020). North American cold events following sudden stratospheric warming in the presence of low Barents-Kara Sea sea ice. *Environmental Research Letters*, *15*(12), 124017. https://doi.org/10.1088/1748-9326/abc215

Zhang, P., Wu, Y., Simpson, I. R., Smith, K. L., Zhang, X., De, B., & Callaghan, P. (2018). A stratospheric pathway linking a colder Siberia to Barents-Kara Sea sea ice loss. *Science Advances*, *4*(7), eaat6025. https://doi.org/10.1126/sciadv.aat6025

Zhu, Y., & Newell, R. E. (1998). A proposed algorithm for moisture fluxes from atmospheric rivers. *Monthly Weather Review*, *126*(3), 725–735. https://doi.org/10.1175/1520-0493(1998)126<0725:APAFMF>2.0.CO;2